J Mol Model (2013) 19:5545–5559
DOI 10.1007/s00894-013-2042-2

ORIGINAL PAPER

QM-MM simulations on p53-DNA complex: a study of hot spot and rescue mutants

Shruti Koulgi · Archana Achalere · Neeru Sharma · Uddhavesh Sonavane · Rajendra Joshi

Received: 4 July 2013 / Accepted: 21 October 2013 / Published online: 21 November 2013
© Springer-Verlag Berlin Heidelberg 2013

Abstract p53 is a transcription factor involved in the expression of a number of downstream genes in response to genotoxic stress. It is activated through post translation modifications in normal as well as cancerous cells. However, due to mutations occurring in p53 in cancer cells it is not able to perform its function of DNA binding which leads to cell proliferation. It is found to be mutated in 50 % of the cancers. These mutations occur at a high frequency in the DNA binding region of the p53. Among the known seven hot spot cancer mutations G245S, R249S, and R273C have been studied here using quantum mechanics and molecular mechanics (QM-MM) simulations. These mutations along with their experimentally proven rescue mutations have also been included in the present work. A comparative study of these cancer mutations along with wild type and their rescue mutations has been performed. A computational measure based on the free energy changes occurring in the binding of the p53 to the DNA has been presented. A correlation between the DNA binding property and important interaction between p53 and DNA has been observed for all the mutants. The keys residues which contribute to the binding of p53 to DNA by forming crucial hydrogen bonds have also been discussed in detail. A 30 ns simulation study was analyzed to observe the local structural changes and DNA binding property of p53 in case of wild type, cancer and rescue mutants.

Keywords Free energy · p53-DNA complex · QM-MM simulations · Rescue mutations

Electronic supplementary material The online version of this article (doi:10.1007/s00894-013-2042-2) contains supplementary material, which is available to authorized users.

S. Koulgi · A. Achalere · N. Sharma · U. Sonavane · R. Joshi (✉)
Bioinformatics Group, Centre for Development of Advanced Computing (C-DAC), Pune University Campus, Pune, India 411 007
e-mail: rajendra@cdac.in

Introduction

The transcription factor p53 is a tumor suppressor protein which is involved in up-regulation of various genes under stress conditions such as DNA damage and many others. It normally functions in the cellular processes such as cell cycle arrest, DNA repair and apoptosis [1, 2]. On the other hand reduction or elimination of the p53 activity is characteristic of more than half of all human cancers. One of the major causes in reduction of p53 activity is associated with its mutations [3, 4]. Most of these mutations occur in the sequence-specific DNA binding core domain [4–6]. In the recent past there has been a lot of progress on cancer therapies that target p53 mutants for drug intervention of tumors [7].

p53 is a 393 residue long protein which functions as a tetramer to perform DNA binding. Each monomer interacts with the DNA through the zinc co-ordination complex. The monomer consists of multiple domains performing different roles in the cellular processes. The N-terminal and C-terminal domains are the regulatory domains of p53 [8]. The core domain of p53 is the largest domain consisting of approximately 200 residues and performs the function of DNA binding, therefore known as the DNA binding domain (DBD). p53 performs the DNA binding activity in association with zinc ion which forms a tetrahedral co-ordination complex with CYS 176, CYS 238, CYS 242, and HIS 179. The DBD comprises two regions viz. minor and major groove binding regions (Fig. 1a). The major groove binding region consists of a loop-sheet-helix motif and the minor groove binding region is comprised of two large loops and the zinc co-ordination complex. This co-ordination complex is important in order to maintain the integrity of DBD. The p53 is known to aggregate in the absence of zinc ion. The zinc co-ordination complex when assisted by the two large loops L2 and L3 (Fig. 1a) strengthens the DNA binding interaction via the minor groove of the DNA [9, 10]. The zinc ion plays a crucial role in

providing stability to these loops as well as neighboring loops and also has an effect on the DNA-binding specificity [9, 10]. This DBD is highly susceptible to mutations [11–13] which cause key structural changes further leading to inactivation of p53 in more than 50 % of all human cancers [13–15]. There are seven hot spot residues which have been identified as the sites where highest frequency of mutations occur [16]. All these mutations are broadly classified as structural and contact mutations depending on their physical locations within the protein. The structural mutations cause structural perturbations that destabilize the DBD surface which gives rise to loss of DNA binding. The contact mutations are known to affect DBD through loss of residues that are directly involved in p53-DNA interactions. Among the seven hot spot mutations R175H, Y220C, G245S, R249S, and R282W are known as structural mutations and the remaining two R248Q and R273C come under the class of contacts mutations (Fig. 1b).

The effect of these cancerous or oncogenic mutations on the DNA binding property and structural integrity has been of major research interest in the last few years. The analysis and understanding of mutation effects on p53 functioning may help in designing of drug molecules that may restore the p53 activity. Use of such drugs in cancer therapy is of current clinical research interest [17–19]. Cancerous mutations are also known to destabilize the protein by inducing loss of local structures, as the stability of p53 is governed by its DNA binding domain. Experimental studies have reported analysis of thermodynamic instability of wild type and mutant p53 [20–23]. However, the stability of the mutant p53 DNA binding domain can be regained by inducing certain mutations widely recognized as second site suppressors. In order to confront the oncogenic mutations various reactivation strategies have been designed. These strategies include exogenous expression of p53 via adenovirus mediated gene transfer [24, 25], restoration of function by introducing second site suppressor mutations [26–31]. However, intragenic second site suppressors have been extensively studied through *in vivo* and *in silico* experiments as these methods provide mechanistic insights into possible ways of rescuing mutant p53. Experiments like yeast genetic approach [27, 30], NMR spectroscopy [28] and X-ray crystallography [32–34] have given an insight on reactivation mechanism using second site suppressor mutations for p53 mutants. Profound data has been made available on diverse structural and functional consequence of mutation to understand the structure-function-rescue mechanism of p53 cancer mutant [35].

In-silico methods such as molecular dynamics (MD) simulations complements experimental understanding by providing local structural and dynamical insights of functioning of wild type and mutant p53. MD simulations have been performed to study structural and dynamic properties of the p53, DNA binding domain [36–38]. Although, only few MD simulations on p53-DNA wild type complex and its mutational effects have been reported till date [36, 39, 40]. Free energy calculations through MD simulations are reported to identify loss and rescue of DNA binding to p53 core domain by single and double mutations [39, 40]. One of the recent MD simulations on the p53 monomer, depicts a computational metric which helps to determine the functionality of a particular p53 mutant [41]. The metric derived was based on the number of

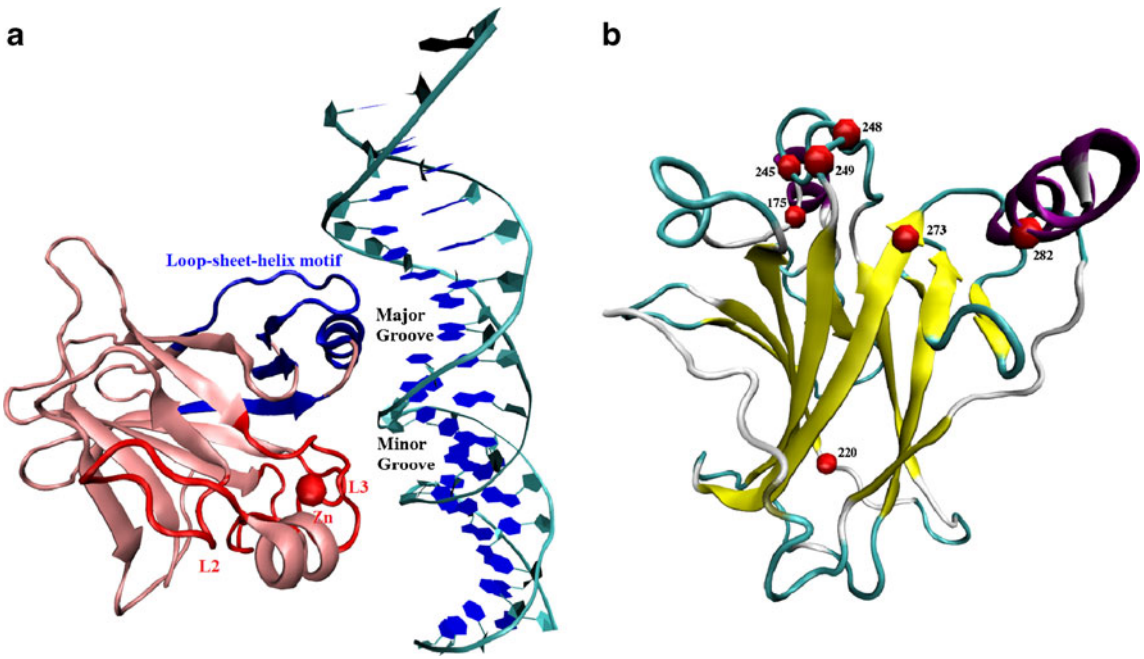

Fig. 1 PDB ID: 1TSR chain B with double stranded DNA. Loop-sheet-helix region (blue) binds major groove. Large loop L2, L3 and the zinc ion(red) binds minor groove (**a**) and position of the seven hot spot residues (red spheres(**b**))

clusters (NOC) derived using RMSD cut-off which were further correlated to the protein stability and functionality [41]. This study also indicates that at least 30 ns simulation is required to predict the functionality of the p53 mutants. The loss or gain of functionality was based on NOC calculated for each mutant. As NOC is dependent on the RMSD cut-off, it attributes to the structural rearrangements occurring in the protein overall. However, the effect on functionality of the p53 molecule may be more effectively understood by computing the binding property of p53 with DNA in addition to measuring the stability of p53 alone. The reason being, most of the experimental studies report loss of DNA binding in case of the p53 mutants.

In the current study, the prime objective was to develop a measure using the computed free energy of binding of p53 toward DNA and correlate it with crucial interactions formed between the two. The higher value of free energy of binding suggests unstability in DNA binding of p53 and vice versa. The zinc co-ordination complex is very important for DNA binding of p53 as explained earlier [9, 10]. Classical MD simulations prove to be challenging in sustaining this complex. In the past, different strategies like dummy atom, bonded and modified force field approach have been used for maintaining the zinc co-ordination complex in MD simulations of p53-DNA complex [36, 40, 41]. Similarly, in the current study an attempt was made to preserve this complex by treating it with quantum mechanics (QM) and not applying any restraints. Performing QM on such an important functional entity of the protein would help in mimicking the actual biological behavior [42]. Hence, maintaining the zinc co-ordination complex was the sole objective of introducing the quantum treatment. Quantum and molecular mechanics (QM-MM) simulations were performed on the DNA bound p53 complex for the wild type and three of the hot spot mutations viz. G245S, R249S, and R273C. A rescue mutant for each of these oncogenic mutations was also studied. The detailed description of QM-MM simulations has been discussed in methodology.

G245S and R249S are the structural mutations of p53 which reside in the loop region of the p53 DBD. The G245S is known to be rescued by the H178Y second site suppressor mutation [43]. MD simulations on the p53 monomer with G245S mutation have been reported in the past [41] but not for mutant G245S along with the H178Y rescue mutant. R249S is known to be rescued by T123A in combination with H168R, a double second site suppressor mutation [28–31]. This triple mutant has been extensively studied through experimental techniques but no MD simulation study has been performed till date. R273C which comes under the class of contact mutations leads to major loss in DNA binding activity of p53 with very little structural changes. T284R is considered to rescue this oncogenic mutant [8, 34, 35, 39, 40]. MD simulations on R273C alone have been performed in the past but not in combination with this rescue mutant [40]. All these mutations have been extensively studied through experimental techniques but few MD simulation studies have been performed. Performing MD simulations would give an idea about the structural changes occurring in this mutant leading to its rescue nature.

Overall seven QM-MM simulations have been performed which comprised of DNA bound p53 wild type, three cancer mutants (G245S, R249S, R273C) and three rescue mutants (*G245S_H178Y*, *R249S_T123A_H168R*, *R273C_T284R*) for 30 ns each. The simulations have been categorized as given in Table 1. The correlation between the free energy of binding and crucial interactions between p53 and DNA was obtained. The key residues involved in contributing toward the DNA binding property of p53 have also been highlighted in the present study. The measure proposed in the current work may help to identify the cancerous or rescue nature of any mutation in p53 that needs to be scrutinized.

Materials and methods

System preparation

The coordinates for the starting structure were obtained from chain B and complete double stranded DNA of PDB ID 1TSR [12]. Each cancer and rescue mutant was prepared from this structure using the *xleap* module of AmberTools 1.5 [44]. The zinc ion was present in a tetrahedral coordination complex with CYS 176, HIS 179, CYS 238, and CYS 242. The distances and angles required for the formation of the tetrahedral complex were obtained from the work reported by Lu et al. in the year 2007 [36]. The entire p53-DNA-zinc complex was initially neutralized by adding Na+ions followed by explicit solvation using the TIP3P water model [44]. The topology and coordinates were generated using the Amber FF03 force field [44]. The system size for the wild type and other p53 variants was approximately 63300 atoms.

QM-MM simulations

In each of the solvated p53-DNA systems the zinc co-ordination complex was treated using the quantum

Table 1 The table describes the mutants considered for the simulations

Simulation	p53 variant	Mutation type
WT	Wild type	-
CM1	G245S	Cancer
RM1	*G245S_H178Y*	Rescue
CM2	R249S	Cancer
RM2	*R249S_T123A_H168R*	Rescue
CM3	R273C	Cancer
RM3	*R273C_T284R*	Rescue

mechanical (QM) method. The entire simulation system except for the zinc co-ordination complex has been considered for molecular mechanics (MM) simulations. Therefore, all the minimization, temperature ramping, equilibration and production run protocols follow a QM-MM method. The PM3 method [45] was employed for the QM region whereas, the Amber FF03 force field was applied to the MM region [44]. The overall charge of the QM region was considered to be +2 attributing to the charge on the zinc ion. The bonds containing hydrogen atoms in the QM and MM region were constrained using the SHAKE algorithm [46]. The canonical ensemble, NVT was applied, where the number of atoms, box volume, and the temperature of each of the system were maintained throughout the simulation [47]. The QM-MM interface was treated according to the link atom approach as described by Walker et al. [48–50]. The default parameters for the link atom approach were used in the current study. The time step was considered to be 2 fs with temperature maintained at 300 K using Langevin dynamics and a collision frequency of 0.1 ps^{-1} [47]. The periodic boundary conditions (PBC) were applied to perform the constant volume dynamics. The particle mesh Ewald (PME) method was employed with a non-bonded cut-off of 12Å. The minimization was performed in two stages. First, the solvent was minimized using the steepest descent method for 20,000 steps. Next, the p53-DNA-Zn complex was released and the minimization was performed for 50,000 steps. The temperature was increased up to 300 K for the solvent in 40 ps followed by the p53-DNA-Zn complex in the next 40 ps. The equilibration was performed for 2 ns. The production run was carried out till 30 ns. The Amber 10 simulation package was used for all the simulations. Overall seven QM-MM simulations were performed comprising the wild type p53, three cancer mutants and their corresponding rescue mutations resulting in an overall simulation time of 210 ns. The cancer mutants included two structural mutations, G245S and R249S and one contact mutation, R273C (Table 1). The rescue mutants for the same were *G245S_H178Y*, *R249S_T123A_H168R*, and *R273C_T284R* respectively (Table 1).

Analysis performed

The analysis was performed using AmberTools 1.5 [44] on trajectories having snapshots at every 10 ps interval from a simulation of 30 ns. Free energy values were calculated using the *mm-pbsa* module of AmberTools 1.5. This module is efficient in calculating the free energy for the entire system as well as the contribution of free energy made by the individual residues of the system. This module has both molecular mechanics-generalized Born surface area (MM-GBSA) and molecular mechanics-Poisson-Boltzmann surface area (MM-PBSA) methods which calculate the binding free energies for macromolecules by combining molecular mechanics calculations and continuum solvation models. The following equation was used to calculate the change in free energy of binding,

$$\Delta\Delta G_{bind} = \Delta G_{complex(com)} - \left(\Delta G_{receptor(rec)} + \Delta G_{ligand(lig)}\right) \quad (1)$$

$$\Delta G_{com/rec/lig} = < \Delta E_{gas(com/rec/lig)} > + < \Delta G_{sol(com/rec/lig)} > - T < \Delta S_{com/rec/lig} > \quad (2)$$

,

where $\Delta E_{gas(com/rec/lig)}$ is a molecular mechanics energy, $\Delta G_{sol(com/rec/lig)}$ is the solvation energy calculated either by solving Poisson's equation (PB) or by using generalized Born (GB) solvation model. $T\Delta S_{(com/rec/lig)}$ is the entropy contribution to the free energy $\Delta G_{(com/rec/lig)}$ of the molecule [44] [51].

The 3000 snapshots generated at every 10 ps from a 30 ns trajectory were used to calculate the change in free energy of binding ($\Delta\Delta G_{bind}$) of the complexes using the MM-GBSA method. The p53 molecule was considered as the receptor and the double stranded DNA was considered as the ligand. Thus, $\Delta\Delta G_{bind}$ depicts the change in free energy of binding between p53 and DNA. However, in this case only the terms $<\Delta E_{gas(com/rec/lig)}>$ and $<\Delta G_{sol(com/rec/lig)}>$ were calculated. The reason being, calculating the term T $<\Delta S_{com/rec/lig}>$ for 3000 snapshots of seven simulations would prove to be computationally very intensive. Although, in order to check the effect of T $<\Delta S_{com/rec/lig}>$, it was calculated every nanosecond (ns) resulting in 30 snapshots. All the plots of $\Delta\Delta G_{bind}$ shown in the results consider only $<\Delta E_{gas(com/rec/lig)}>$ and $<\Delta G_{sol(com/rec/lig)}>$. The results considering T $<\Delta S_{com/rec/lig}>$ have been reported in the Supplementary material. T $<\Delta S_{com/rec/lig}>$ was calculated using the normal mode analysis program present in the *mm-pbsa* module [44]. The choice of MM-GBSA method for free energy calculation proves to be computationally more efficient as compared to other methods such as free energy perturbation (FEP) and thermodynamic integration (TI) [51]. Owing to the large size of the data set (3000 conformations) MM-GBSA proves to be the best option for free energy calculation. The number of hydrogen bonds were calculated using *cpptraj* [44]. The strength of any particular hydrogen bond was estimated by calculating the percentage occupancy of the same throughout the simulation. The percentage occupancy refers to the percentage of number of frames in which a particular hydrogen bond is formed out of the total number of frames (3000). The free energy value for residues was calculated using the residue-wise decomposition method present in MMPBSA.py module of AmberTools 1.5 [44]. The free energy value for every residue was averaged over the entire trajectory of 30 ns.

To monitor whether the simulated systems attained equilibrium during the production runs, few essential parameters

like total energy, temperature, root mean square deviation (RMSD) and radius of gyration were plotted. The data for the same have been provided in the Supplementary material (Fig. S1 and S2).

Results and discussion

Free energy of binding and hydrogen bonding between p53 and DNA

In order to understand the DNA binding activity of p53 variants, the change in free energy of binding ($\Delta\Delta G_{bind}$) and the number of hydrogen bonds (NOH) formed between p53 and DNA were calculated. The NOH formed was calculated using the *cpptraj* module of AmberTools 1.5 where, the cut-off for donor-acceptor bond distance and angle were 3 Å and 135° respectively [44].

Linear regression analysis was performed by considering NOH as the independent and $\Delta\Delta G_{bind}$ as the dependent variable. The line of regression explains the trend followed by the two, dependent and independent variables. The distribution of each of the data set lies in the vicinity of the line of regression. This linear regression analysis was performed on all the p53 variants.

Figure 2a describes the linear regression analysis performed on the wild type (WT in black), G245S (CM1 in red), and *G245S_H178Y* (RM1 in green). The $\Delta\Delta G_{bind}$ and NOH were found to be negatively correlated. The line of regression for WT shows that the major distribution lies in the range of −70 to −50 kcal mol^{-1} of $\Delta\Delta G_{bind}$ values which indicates stable binding between p53 and DNA. However, the major distribution for $\Delta\Delta G_{bind}$ values of CM1 laid in the range of −60 to −37 kcal mol^{-1}. This higher $\Delta\Delta G_{bind}$ range implies unstable or weak binding of DNA in CM1 as compared to WT. On the other hand, the major distribution for $\Delta\Delta G_{bind}$ values of RM1 was observed in the range −75 to −50 kcal mol^{-1} which is comparatively lower than both WT and CM1. This indicates that RM1 showed strong binding activity as compared to CM1.

Figure 2b describes the linear regression analysis performed on R249S (CM2 in red) and *R249S_T123A_H168R* (RM2 in green). The major distribution for $\Delta\Delta G_{bind}$ of CM2 laid in the range of −55 to −35 kcal mol^{-1} which was quite a bit higher than that observed in WT. This infers that the DNA binding activity had declined in CM2 as compared to WT. However, a part of the distribution of $\Delta\Delta G_{bind}$ for RM2 was observed in the range of −75 to −60 kcal mol^{-1} which is closer to WT. This indicates that there was a gain in the DNA binding activity of RM2 which was absent in the case of the CM2.

Figure 2c describes the linear regression analysis performed of R273C (CM3 in red) and *R273C_T284R* (RM3 in green). The complete distribution of $\Delta\Delta G_{bind}$ for CM3 laid in the range of −46 to −36 kcal mol^{-1} which shows similar behavior as CM2. This suggests that the DNA binding activity was also hampered in CM3 as compared to WT. Whereas, for RM3 the distribution of $\Delta\Delta G_{bind}$ spans a large range of −70 to −32 kcal mol^{-1}. This shows there was a gain in the DNA binding activity of RM3 which was not observed in the case of the CM3. Hence, the RM3 had better DNA binding activity as compared to CM3.

This linear regression analysis states that in cancer mutants, all the conformations in 30 ns long simulation lie in the region of higher $\Delta\Delta G_{bind}$ values as compared to WT which affirms lower stability in binding. However, in rescue mutants two instances were observed. First, either all the conformations lie in the region of lower $\Delta\Delta G_{bind}$ (Fig. 2a) and second they partially lie in the region of higher and lower $\Delta\Delta G_{bind}$ (Fig. 2b and c) as compared to WT. In the second situation the slope of the line of regression is higher as compared to that of the wild type and cancer mutant. As discussed in the methodology linear regression analysis was also performed considering T $\Delta S_{(com/rec/lig)}$ for 30 snapshots (every nanosecond). It was observed that all the cancer mutants laid in the

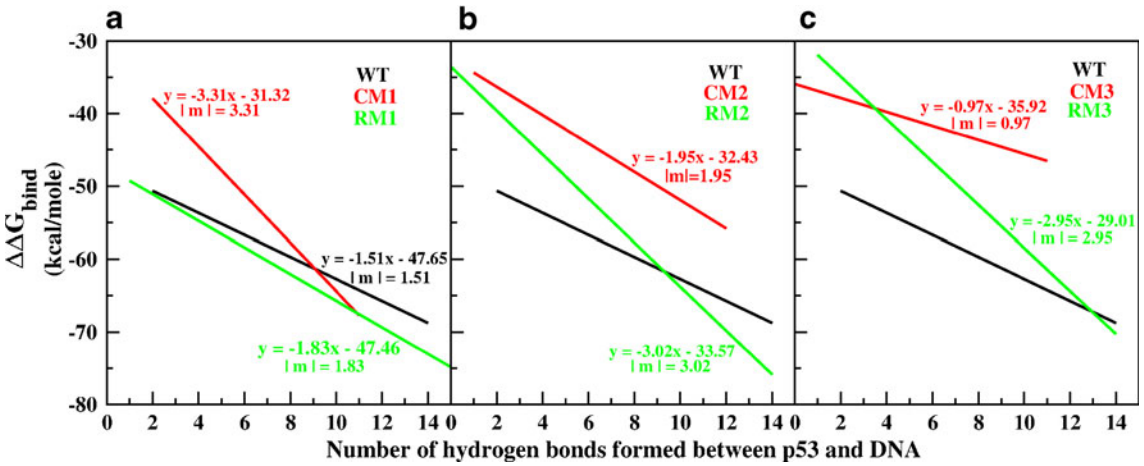

Fig. 2 The correlation between the $\Delta\Delta G_{bind}$ and number of H-bonds (NOH) between p53-DNA for Glycine 245 (**a**),Arginine 249 (**b**), and Arginine 273 (**c**)

region of higher $\Delta\Delta G_{bind}$ values as compared to wild type and their rescue mutants (Supplementary Data: Fig. S3) . Although, the slopes of the lines differ attributing to the small data set of just 30 snapshots. This indicates that in order to transit from unstable to stable binding region the rescue mutants undergo structural changes which help to strengthen the DNA binding activity of the p53 variant. The convergence was evaluated by observing the behavior of averaged binding free energy of each complex with respect to time (Fig. S6).

Interface residues between p53 and DNA

The DNA binding activity of p53 involves different non-bonded interactions between the p53 and DNA residues. There are a few interface residues of p53 which participate in hydrogen bonding with the DNA. A detailed study on behavior of these interface residues was performed by calculating the hydrogen bonds formed between them and the DNA.

Hot spot residue: glycine 245

Figure 3a represents the number of hydrogen bonds (H-bonds) formed between the interface residues of p53 and DNA of WT, CM1, and RM1. These hydrogen bonds considered were stable for at least 5 ns, which corresponds to 20 % occupancy. It was observed that in the case of WT there were 11 such H-bonds formed. These 11 H-bonds were considered as a reference for comparison with cancer and rescue mutants. Overall, eight interface residues from the WT viz. SER 121, THR 123, ASN 239, SER 241, ARG 248, ARG 273, ALA 276, and ARG 280 were involved in hydrogen bond formation. Except for ARG 248, ARG 273, and ARG 280 the rest of the five residues formed single hydrogen bond whereas these three formed two H-bonds each. ARG 248 forms one hydrogen bond with thymidine (Thy) 35 (ARG 248^1) and another with guanine (Gua) 34 (ARG 248^2). ARG 273 forms one with O1P atom of Thy 12 (ARG 273^1) and another with O5' atom (ARG 273^2) of the same DNA residue. ARG 280 forms one with O6 atom of Gua 13 (ARG 280^1) and another with N7 atom (ARG 280^2) of the same DNA residue. In the case of CM1 eight H-bonds were formed out of which only three were identical to those formed in WT. Whereas, in RM1 a total of 14 H-bonds were formed out of which, eight were identical to those formed in WT. This figure explains that, in case of RM1 there were more number of H-bonds that matched with WT as compared to that of CM1. The total number of interactions between p53 and DNA with respect to hydrogen bonding was highest in RM1 (*G245S_H178Y*) followed by WT (wild type) and CM1 (G245S).

Figure 3b represents the comparison of the occupancy of the matched H-bonds between WT, CM1, and RM1. In CM1, two H-bonds (SER 241 and ARG 273^1) out of the three identical to WT showed occupancy less than WT. The remaining one showed more occupancy than both WT and RM1. The five H-bonds that are unmatched with WT have been listed in Table 2. SER 121, ARG 273, and ARG 280 were involved in formation of these H-bonds. On the other hand in RM1, out of the eight matched H-bonds six (ASN 239, ARG 248^1, ARG 248^2, ALA 276, ARG 280^1, and ARG 280^2) showed similar occupancy levels to that of WT with range between 20 to 70 %. The remaining two (SER 241 and ARG 273^1) showed occupancy levels less than WT. The six unmatched H-bonds (Fig. 3a) have been listed in the Table 2. In RM1, other than ARG280, two additional residues THR118 and ALA 119 were found to participate in the formation of hydrogen bond.

Figure 3c represents the contribution made by the interface residues in binding in terms of free energy for WT, CM1, and RM1. In CM1, five residues (THR 123, SER 241, ARG 248, ARG 273, and ALA 276) showed higher free energy as compared to WT which infers that the binding activity was reduced in these interface residues. Although, in CM1 it was also observed that three residues (SER 121, ASN 239, and ARG 280) showed better binding as compared to WT and RM1. This can be attributed to the fact that SER 121 formed two (Table 2) and ASN 239 formed one (Fig. 3b) stronger H-bond than WT and RM1. In the case of ARG 280, the average bond distance of the H-bonds formed in WT and RM1 was 2.8 $\AA$ whereas in CM1 it was 2.0$\AA$. However in RM1, five interface residues showed better binding as compared to CM1. Apart from these five, the two interface residues THR 118 and ALA 119 which formed novel H-bonds showed better binding than WT and CM1. Thus, it can be inferred that more stable binding is observed in the interface residues of RM1 as compared to that of CM1 in terms of both hydrogen bond occupancy and free energy contribution.

Hot spot residue: arginine 249

Figure 4a represents the number of H-bonds formed between the interface residues of p53 and DNA with occupancy more than 20 % for WT, CM2, and RM2. CM2 formed four such H-bonds out of which only one was identical to WT. Whereas, in the case of RM2 nine such H-bonds were formed with five identical to WT. Thus the figure explains that RM2 (*R249S_T123A_H168R*) shows better hydrogen bonding with DNA than CM2 (R249S), as a larger number of H-bonds match with WT.

Figure 4b explains the comparison of % occupancy of the matched H-bonds between WT, CM2, and RM2. The residue at 123rd position is referred to as X, as it is threonine (THR) in WT and CM2 and alanine (ALA) in the case of RM2. CM2 formed only a single hydrogen bond (ALA 276) identical to WT which had occupancy less than both WT and RM2. The remaining three unmatched H-bonds (Fig. 4a) listed in Table 3 belonged to the interface residues SER 121, ASN 239, and

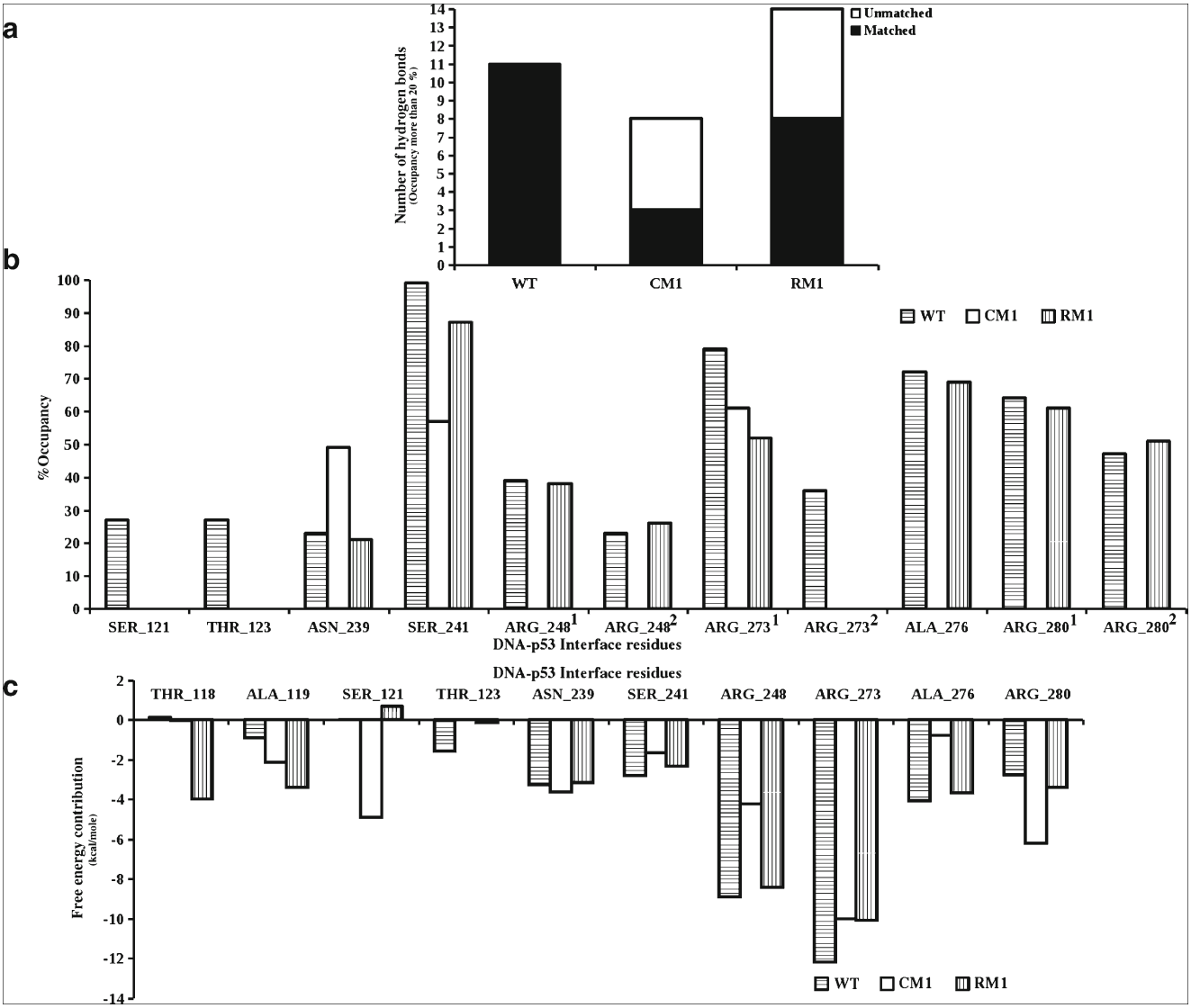

Fig. 3 Number of H-bonds formed between p53-DNA (**a**), occupancy of the matched H-bonds(**b**) and free energy contribution made by interface residues(**c**) for Glycine 245

ARG 280. However, RM2 formed five H-bonds identical to WT out of which two (ARG 280^1 and ARG 280^2) showed occupancy greater than WT within the range of 45–70 %. The remaining three (SER 241, $ARG273^1$ and ALA 276) had occupancy lower than WT. The four unmatched H-bonds (Fig. 4a) are listed in Table 3. In RM2, in addition to SER 121 two other residues LYS 120 and ARG 283 were involved in hydrogen bond formation.

Figure 4c depicts the contribution made by the interface residues in binding in terms of free energy for WT, CM2, and RM2. In CM2, five interface residues (THR 123, SER 241, ARG 273, ALA 276, and ARG 283) showed free energy higher than WT which infers that the binding was affected in them. Although, in CM2 there were few residues which showed better binding stability. LYS 120 showed the most stable binding in CM2 followed by RM2 and WT. The difference between the free energy values between CM2 and RM2 was less that 1 kcal mol^{-1}. However in RM2, LYS 120 formed a single hydrogen bond with 23 % occupancy (Table 3). SER 121 had the most stable binding activity in CM2 followed by WT and RM2. This residue formed a single hydrogen bond in CM2 with occupancy 35 % which was greater than the one formed in WT and RM2 (28 %). ARG 248 had the most stable binding activity in CM2 followed by WT and RM2. As the hydrogen bonding was better in WT as compared to CM2 other interactions of ARG 248 were observed. The number of contacts made by this residue with the DNA within a cut-off of 3.5$\AA$ were calculated. The results showed that from the start of the simulation the CM2 had a larger number of contacts as compared to WT and RM2 (Supplementary data: Fig.S4). This property can be attributed to the fact that when averaged over the entire simulation ARG 248 showed more stable binding in CM2 as compared to WT and

Table 2 The table describes the unique (unmatched) H-bonds (more than 20 % occupancy) formed by CM1 and RM1

DNA residue	p53 residue	Occupancy (%)
	CM1	
DT12@O2P	ARG273@HH22	86
DG28@O2P	SER121@H	85
DG28@O2P	SER121@HG	81
DG29@O2P	ARG280@HH11	31
DG30@O6	ARG280@HH22	21
	RM1	
DT26@O1P	THR118@HG1	44
DT26@O2P	THR118@H	43
DT26@O2P	ALA119@H	34
DT26@O1P	THR118@H	26
DT12@O1P	ARG280@HH22	22
DT26@O2P	THR118@HG1	21

Table 3 The table describes the unique (unmatched) H-bonds (more than 20 % occupancy) formed by CM2 and RM2

DNA residue	p53 residue	Occupancy (%)
	CM2	
DT12@O2P	SER121@HG	35
DG13@O1P	ASN239@HD22	23
DG13@O2P	ARG280@HH22	25
	RM2	
DG28@O2P	LYS120@H	23
DG28@O6	SER121@HG	28
DG13@O1P	ASN239@HD22	46
DG28@O1P	ARG283@HH22	21

RM2. However, ARG 280 was an exception with most stable binding in CM2 followed by WT and RM2. This residue formed a single hydrogen bond in the case of CM2 and two

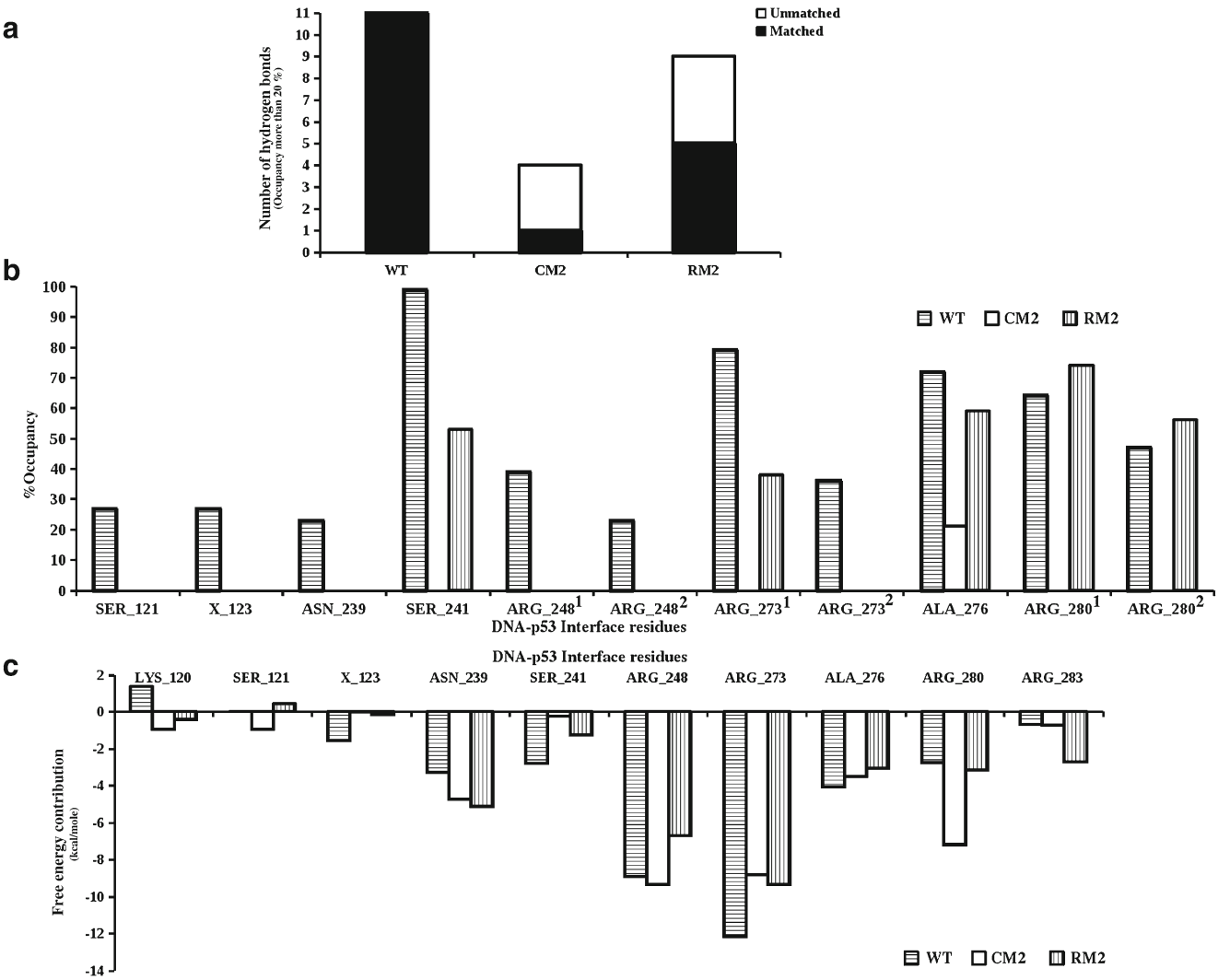

Fig. 4 Number of H-bonds formed between p53-DNA (**a**), occupancy of the matched H-bonds (**b**) and free energy contribution made by interface residues (**c**) for arginine 249 (X=THR in WT & CM2, X=ALA in RM2)

in WT and RM2 each. On the other hand in RM2, four interface residues (ALA 123, ASN 239, SER 241, ARG 273) showed better binding as compared to CM2. Other than these four residues, ARG 283 which formed a novel H-bond showed the most stable binding in RM2 as compared to WT and CM2.

Thus, it was observed that RM2 showed better hydrogen bonding and stability in binding as compared to CM2. The contribution made by the interface residues in order to provide stability in binding of p53 molecule was almost similar in both cases. The reason for this can be explained by revisiting Fig. 2b. It was observed that RM2 spanned a range of −75 to −60 kcal mol^{-1} which suggests gradual improvement in the stability of the p53-DNA binding. Hence, the average free energy values of the interface residues showed similar contribution in providing stability to the binding property of p53. However, the second site suppressor mutation RM2 (*R249S_T123A_H168R*) proved to rescue the DNA binding of CM2 (R249S) by increasing the number of hydrogen bonding interactions.

Hot spot residue: arginine 273

Figure 5a describes the number of H-bonds formed between p53 and DNA with occupancy more than 20 % in the case of WT, CM3, and RM3. CM3 formed seven such H-bonds out of which five were identical to WT. However, in RM3 nine such hydrogen bonds were formed out of which four were identical to WT. Although, CM3 (R273C) formed more H-bonds identical to WT than RM3, the total number of H-bonds formed was more in RM3 (*R273C_T284R*).

Figure 5b explains the % occupancy of the matched H-bonds formed by WT, CM3, and RM3. In WT the 273rd residue is expressed as X, because in WT it is arginine (ARG) whereas in CM3 and RM3 it is cysteine (CYS). In CM3, out of the five matched H-bonds two (SER 121 and SER 241) showed occupancy lower than WT. The remaining three H-bonds showed occupancy more than WT where difference laid within the range 10–20 %. The H-bonds that were not identical to WT (Fig. 5a) have been listed in Table 4. These H-bonds were formed by the SER 121, ASN 239, and SER 241. In RM3, out of the four H-bonds identical to WT one had (ARG 280^2) occupancy greater than CM3. Two H-bonds showed occupancy slightly lower than CM3 where the difference was around 5 %. There were five H-bonds that were not identical to WT (Fig. 5a) which have been given in Table 4. These bonds were formed by SER 121, ASN 239, SER 241, and ARG 248. ARG 248 is one of the contact residues and it formed hydrogen bond in the case of RM3 and not in CM3. This infers that RM3(*R273C_T284R*) showed better hydrogen bonding as compared to CM3 (R273C).

Figure 5c depicts the contribution made by the interface residues in binding in terms of free energy for WT, CM3, and RM3. It was observed that in CM3, five residues (THR 123, SER 241, ARG 248, CYS 273, and ALA 276) showed higher free energy than WT which indicated that the binding activity of these residues was reduced. However, CM3 had two residues ASN 239 and ARG 280 which showed slightly better binding than WT and RM3 within the range of 1 to 2 kcal mol^{-1}. The reason being ASN 239 formed a single hydrogen bond with occupancy 56 % which was greater than that of WT (21 %, Fig. 5b) and RM3 (23–34 %, Table 4). ARG 280 formed the same number of H-bonds with occupancy varying within 5 %. However in RM3, there were two residues (SER 241 and ARG 248) that showed better binding than CM3. Thus, it could be seen that the interface residues of CM3 (R273C) showed loss in binding whereas the ones in RM3 (*R273C_T284R*) showed gain in binding.

Structural changes in p53 mutants

The mutations in p53 not only affects the DNA binding property but also induces some structural changes. The DNA binding domain (DBD) of p53 is known to be a highly unstable domain which attains stability on binding to DNA and its other protein counterparts. The conformational changes are more prominent in the class of structural mutations. Various different parameters have been analyzed in order to find out the different conformational changes occurred in p53 due to G245S, R249S, and R273C mutations.

G245S mutation is known to bring structural changes in the loop 2 region of the p53 core domain [34]. This loop 2 region is involved in the minor groove binding of the DNA along with loop 3 and the zinc co-ordination complex. To investigate the structural changes occurring in the loop 2 region of p53-DBD, principal component analysis (PCA) was performed on the entire trajectory of 30 ns. PCA was performed using the *ptraj* module of Amber Tools 1.5 [44]. The co-ordinates of the backbone atoms were considered as the reaction co-ordinates for PCA. This technique helps to identify the local motions that dominate a particular form of protein. Figure 6 shows the snapshot from the PCA trajectory for the loop 2 conformation of WT (Fig.6 a), CM1 (Fig. 6b), and RM1 (Fig. 6c) obtained at 0th and 30th ns superimposed on chain B of 1TSR. It was observed that the loop 2 conformation is maintained in the case of WT (blue). Loop 2 undergoes conformational change due to elongation in the case of CM1 (red). However, in RM1 (green) loop 2 tries to regain its conformation like WT instead of elongation.

To support this conformational change in loop 2 of p53, the dihedral angles phi ($\varnothing$) and psi (ψ) for the residues of this loop were calculated. As the loop 2 elongation was observed by end of the simulation the last 10 ns were considered. Figure 7 depicts the four residues in this loop region viz. 178 (HIS in WT and CM1, TYR in RM1), GLU 180, SER 183, and ASP 184 that showed drastic change in both the $\varnothing$ and ψ values. It was observed that for all four residues WT

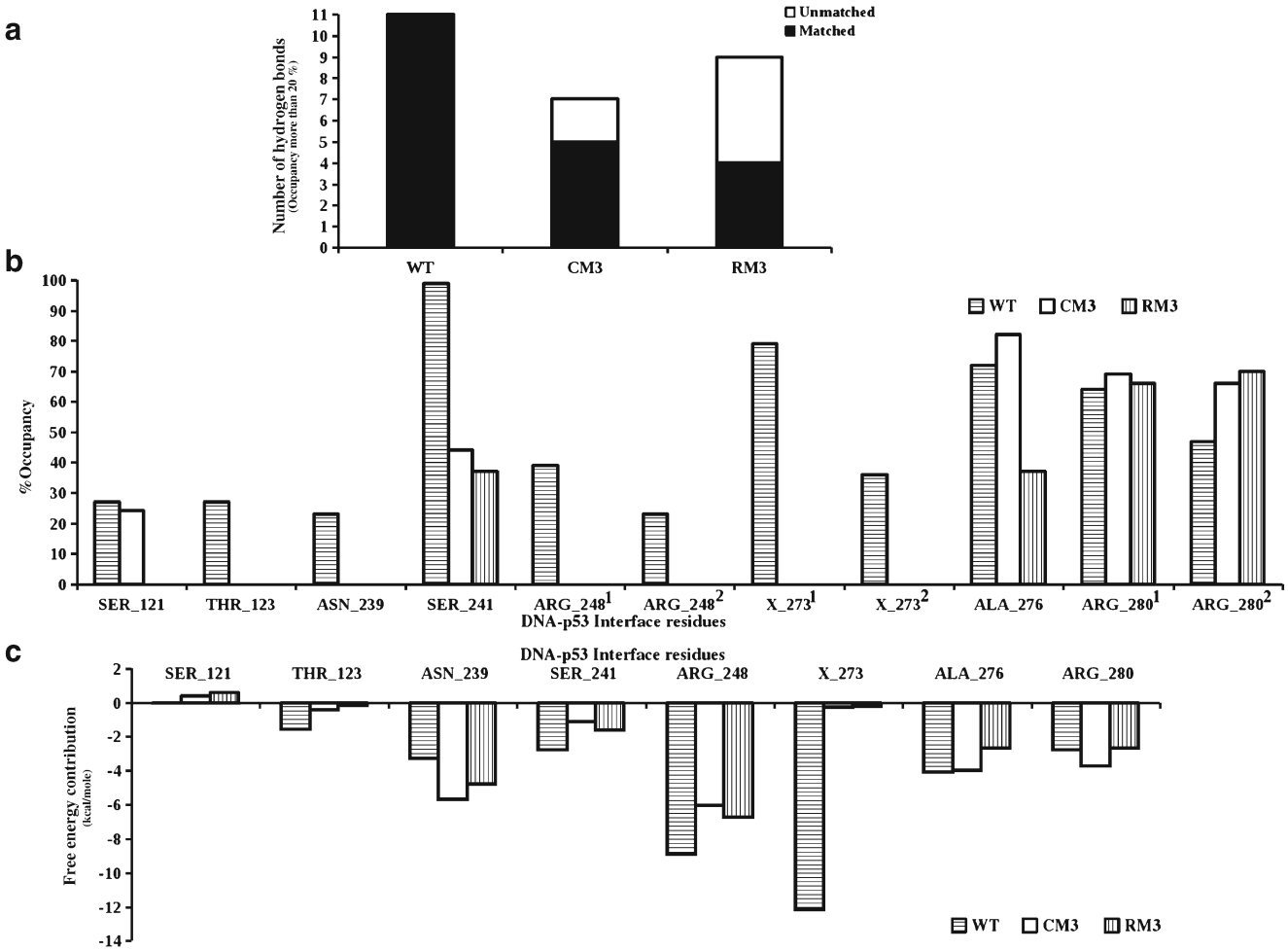

Fig. 5 Number of H-bonds formed between p53-DNA (**a**), occupancy of the matched H-bonds (**b**) and free energy contribution made by interface residues (**c**) for arginine 273 (X=ARG in WT, X=CYS in CM3 & RM3)

and RM1 showed similar values of these dihedral angles whereas it varied distinctly in CM1. However, the residue 178 showed ∅ values (Fig. 7a) within the range of −150° to −60 ° for WT and RM1 but in CM1 it increased to 150° after 25 ns. Similarly, this residue showed ψ values (Fig. 7b) within the range of −30° to 0° for WT and RM1 but in CM1 the values raised to 150° after 25 ns. The 178th residue was the site of rescue mutation in RM1 (*G245S_H178Y*) and helped to revert back the changed conformation of loop 2. Loop elongation was also quantified by calculating the number of H-bonds formed within the loop and RMSD against chain B of 1TSR for the same (Supplementary data: Fig. S5). The drop in the number of H-bonds in CM1 (Fig. S5a) indicates elongation of loop 2 as observed in the PCA calculation. On the contrary, RM1 shows gain in the number of H-bonds. RMSD for loop 2 region increased in CM1 (Fig. S5 B) whereas it was maintained in WT and RM1. These results are in terms with the experimental findings which suggest structural loss in loop 2 region of p53-DBD in G245S [34]. The above results also suggests that RM1 (*G245S_H178Y*) being a rescue mutant helps in rebuilding this structural damage caused by CM1 (G245S).

Table 4 The table describes the unique (unmatched) H-bonds (more than 20 % occupancy) formed by CM3 and RM3

DNA residue	p53 residue	Occupancy (%)
	CM3	
DG28@N7	SER121@HG	24
DG13@O1P	ASN239@HD22	56
DG12@O3'	SER241@HG	26
	RM3	
DG28@O6	SER121@HG	53
DG13@O1P	ASN239@HD22	34
DG13@O2P	ASN239@HD22	23
DG13@O2P	SER241@HG	26
DT12@O1P	ARG248@HE	26

The crystal structure for G245S mutation with PDB ID: 2J1Y is available, which was derived from the superstable quadruple mutant M133L/V203A/N239Y/N268D [34]. However, in the present study only G245S mutation is present.

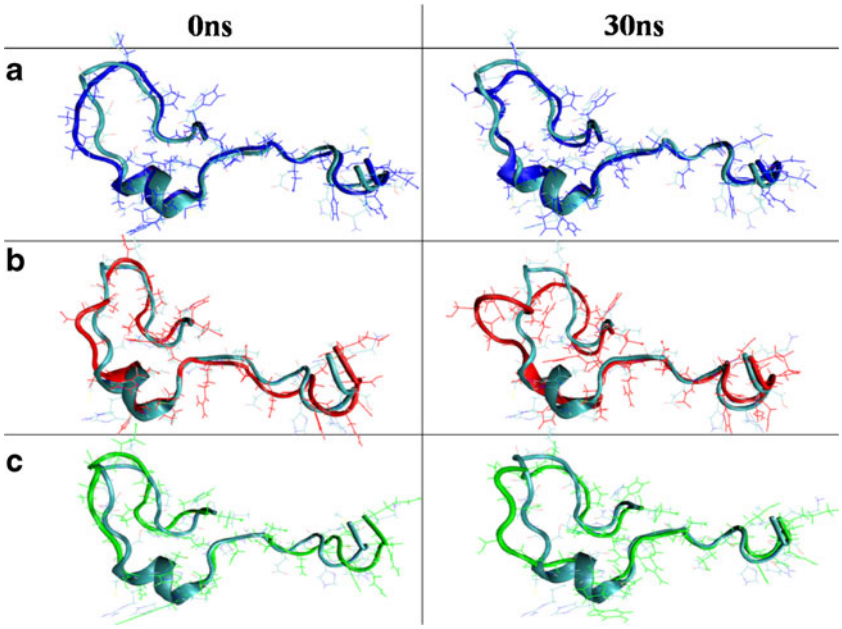

Fig. 6 Loop 2 conformation for WT(**A**), CM1(**B**), and RM1 (**C**) at 0 ns and 30 ns

Backbone RMSD for the entire protein at 30th ns against 2J1Y was 1.454Å, whereas for loop 1, 2, and 3 it was 1.631Å, 1.464Å, and 0.745Å respectively. The RMSD values were observed to be less than 2Å which infers that the conformations obtained through simulations were similar to those seen by experiments.

R249S is another structural mutation of p53-DBD. Arginine is a polar amino acid which is majorly involved in crucial interactions within the protein molecule. In p53, ARG 249 is involved in salt bridge formation with one of the proximal residues GLU 171 [35]. This salt bridge is considered to be one of the important interactions of the p53-DBD. In CM1,

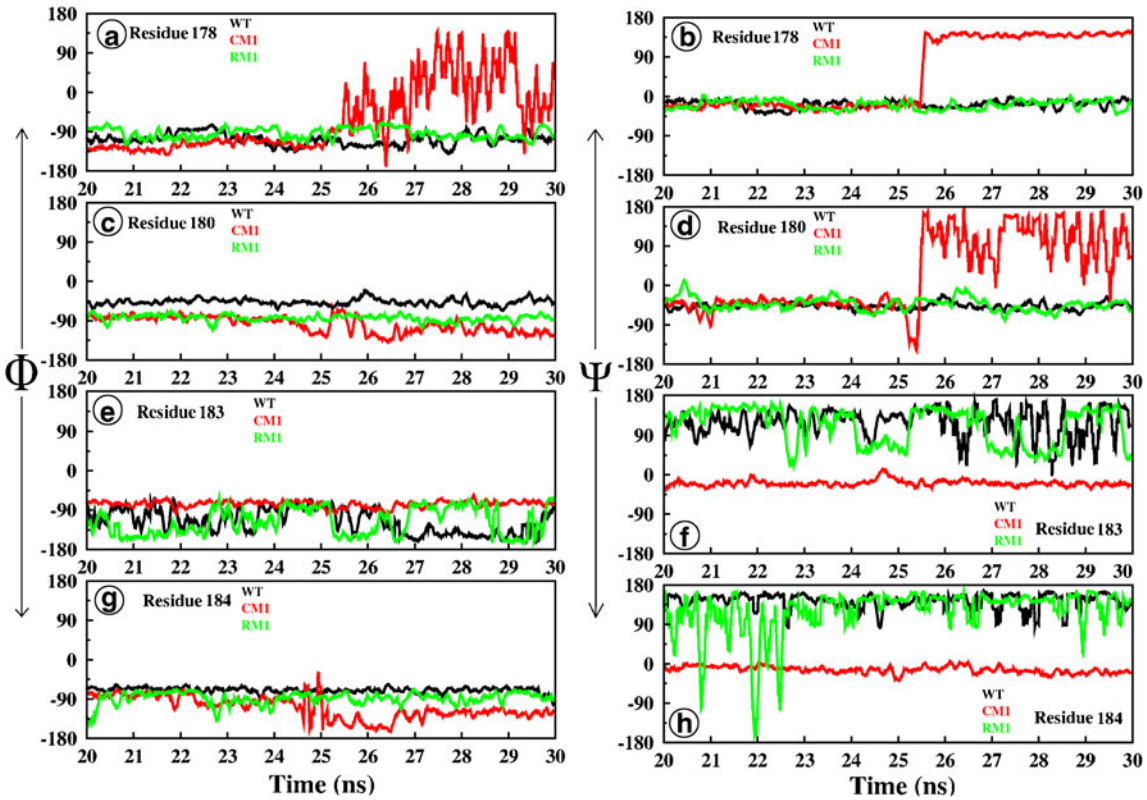

Fig. 7 PHI (∅) (**A**, **C**, E, G) and PSI (ψ) (B, D, F, H) angles for residues 178, 180, 183, and 184 respectively for the last 10 ns

ARG 249 is replaced by SER which is unable to form salt bridge with GLU 171. However, these simulations showed that GLU 171 was not at all involved in any other salt bridge formation in CM2. On the other hand in RM3, ARG 168 which is present in the vicinity of GLU 171 formed a salt bridge with the same. This salt bridge was maintained for more than 20 % of the trajectory. It suggests that the second site suppressor mutation H168R tries to rescue R249S by adding stability to the intra protein interactions. There are studies which report that the free energy of the p53 molecule increases in R249S which makes the molecule more unstable [35]. Table 5 shows the difference in averaged free energy of the p53 molecule for WT, CM2, and RM2. The values of free energy obtained at every nanosecond were considered. The values with and without entropy contribution showed that the rescue mutant RM2 was closer to WT as compared to CM2. R249S being a structural mutation destabilizes the p53-DBD by affecting the loop conformations [31, 35]. The RMSD for the p53-DBD, loop 1, loop 2, and loop 3 of WT, CM2, and RM2 against the chain B of 1TSR has been plotted in Fig. 8. It was observed that the RMSD for CM2 is greater than that of WT and RM2 which shows that the loop conformations are altered in CM2 as compared to WT and RM2. Thus, it can be inferred that the rescue mutation *R249S_T123A_H168R* imparts stability to R249S.

The crystal structure for R249S with PDB ID 3D05 is available [29]. Backbone RMSD of the 30^{th} ns snapshot with that of 3D05 was 1.164Å, whereas for loops 1, 2, and 3 it was 0.228Å, 1.137Å, and 1.839Å respectively. The crystal structure for the rescue mutant *R249S_T123A_H168R* with PDB ID 3D09 is also available [29]. Backbone RMSD of the entire protein at 30^{th} ns snapshot against 3D09 was 1.292Å, whereas for loops 1, 2, and 3 it was 1.539Å, 0.807Å, and 1.066Å respectively. These RMSD values infer that the conformation of R249S and *R249S_T123A_H168R* obtained through simulations was close to the one obtained from experiments.

R273C is one of the contact mutations of the p53 molecule. It majorly leads to the loss of DNA binding activity of p53 without much involvement in structural changes [39]. In p53, ARG 273 forms a salt bridge with ASP 281 which is one of the important interactions to maintain the stability of the protein [34]. In CM3, this ARG 273 is replaced by CYS which is not capable of forming a salt bridge interaction with other residues. Hence, in CM3 ASP 281 does not form any salt bridge with any of the other residues of p53. However, in RM3 ASP 281 forms a salt bridge with ARG 284 which was maintained for more than 40 % of the entire trajectory. These results conclude that the rescue mutation T284R helps to add stability to the p53-DBD by introducing favorable intra-protein interactions. The crystal structure for R273C mutation with PDB ID 2 J20 is available. It was also derived from the superstable quadruple mutant M133L/V203A/N239Y/N268D [34]. In the present study only R273C mutation occurs in the cancer mutant. Backbone RMSD of the entire protein at 30^{th} ns snapshot against 2 J20 was 0.945Å, whereas for loops 1, 2, and 3 it was 1.065Å, 0.519Å, and 1.183Å respectively. These RMSD values may suggest that the conformation of R273C obtained through simulations was similar to the experimentally derived structure.

Table 5 The free energy difference between wild type (WT) and CM2, RM2

p53 variant	Δ (Δ G+T Δ S) (kcal mol^{-1})	Δ (Δ G) (kcal mol^{-1})
Wild type(WT)	0	0
R249S (CM2)	112.5	137.73
R249S_T123A_H168R (RM2)	25.95	−24.03

Temperature sensitive nature of R249S

The hot-spot mutants being explored in the current paper includes R249S, which is known to be a temperature sensitive mutant [52]. The work reported by Friedlander et al. states that R249S (referred to as CM2) shows weak binding to the DNA at 25 °C which futher gets completely abolished at 37 °C [52]. It also includes that in the temperature range of 25–33 °C, CM2 binds weakly to the DNA as compared to WT. Similarly, in the present work the simulations performed at 27 °C showed that DNA binding was weakened in CM2 as compared to WT (Fig. 2b). In order to further investigate the binding at 37 °C, simulations were performed at this temperature for both WT and CM2 for 15 ns each. The last 10 ns were considered for analysis. The comparison of results between 27 °C and 37 °C was done based on the snapshots from 5 to 15 ns. Linear regression analysis similar to that described in the section "Free energy of binding and hydrogen bonding between p53 and DNA" was performed on WT and CM2 at 37 °C. Figure 9a shows the comparison in DNA binding between WT at 27 °C and 37 °C. It was observed that binding occured at both temperatures for WT, which was in acceptance with the work reported by Friedlander et al. [52]. Figure 9b shows the comparison in DNA binding between CM2 at 27 °C and 37 °C. CM2 at 37 °C shows more deterioration in binding as compared to that at 27 °C, which was exactly as reported by Friedlander and coworkers [52]. Figure 9c and d depict the comparison of DNA binding between WT and CM2 at 27 °C and 37 °C respectively. In both cases, CM2 showed loss of binding as compared to WT. Hence, it may be inferred that this correlation works at diffrent temperatures. This can be attributed to the fact, that proper treatment of Zn ion in the QM-MM simulations may have helped to reflect the temperature sensitivity of the p53 mutant. The simulations performed at low and physiological temperatures reflected the temperature sensitive nature of R249S mutant and the

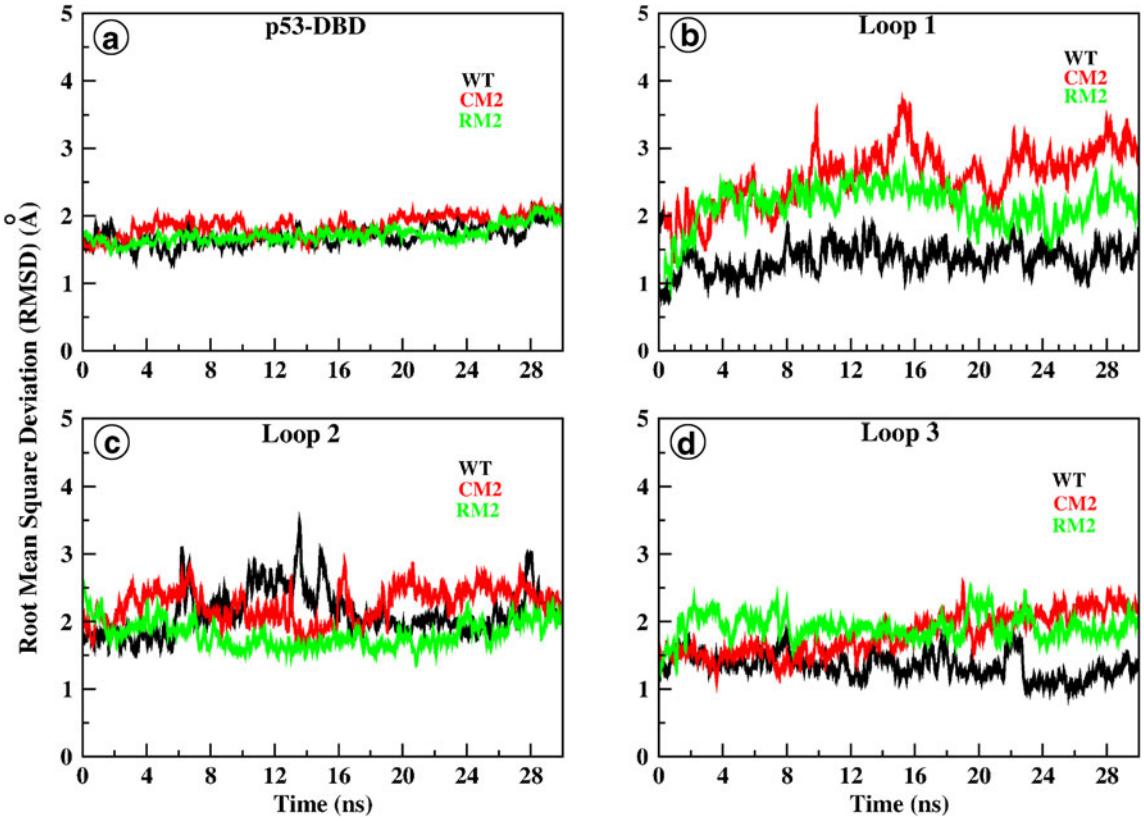

Fig. 8 RMSD of the DNA binding domain (**a**), loop 1 (**b**), loop 2 (**c**), and loop 3 (**d**) of WT, CM2 and RM2 against the chain B of 1TSR

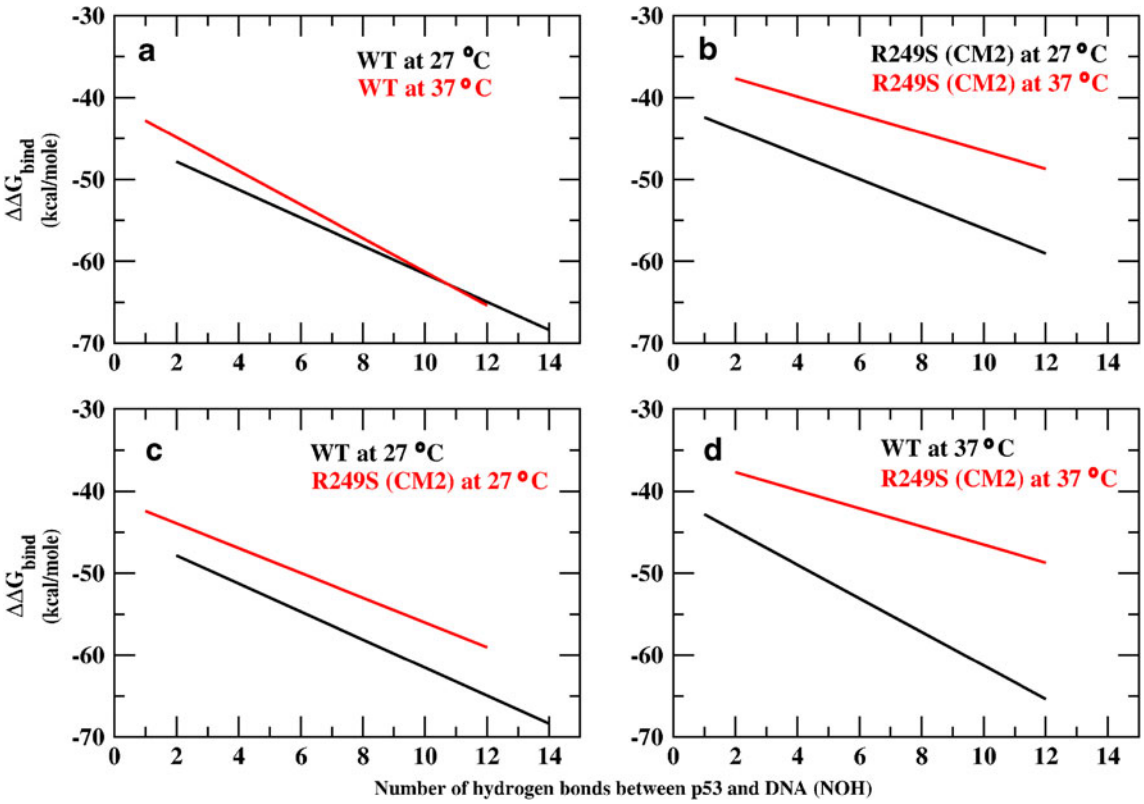

Fig. 9 Comparison of DNA binding between WT at 27 °C and 37 °C (**a**), CM2 at 27 °C and 37 °C (**b**), WT and CM2 at 27 °C (**c**) and WT and CM2 at 37 °C (**d**)

obtained results were in very good agreement with the findings reported by Friedlander et al. [52].

Conclusions

It is prominent that the QM-MM simulations performed on different variants of p53-DNA complex helped to develop an insight into the crucial p53 and DNA interactions, essential to maintain the functional form of p53. The correlation between free energy of binding and hydrogen bonding pattern may prove to be a strong tool to test the DNA binding property of different p53 variants. This correlation could be compared with that seen in the wild type and help to decide whether the p53 variant can be considered as a cancer or a rescue mutant. Although, the experimental efforts play an important role in studying the DNA binding activity of p53. The correlation between $\Delta\Delta G_{bind}$ and NOH obtained through these simulations also prove to be an efficient computational measure to differentiate between the DNA binding property of p53 in the form of cancer and rescue mutations. This measure may also help to capture the temperature sensitive nature of p53 mutants.

Acknowledgments The authors gratefully acknowledge the National PARAM Supercomputing Facility (NPSF) and the Bioinformatics Resources and Applications Facility (BRAF) at Centre for Development of Advanced Computing (C-DAC), Pune, India.

References

1. Vogelstein B, Lane D, Levine AJ (2000) Surfing the p53 network. Nature 408(6810):307–310
2. Vousden KH, Lu X (2002) Live or let die: the cell's response to p53. Nat Rev Cancer 2:594–604
3. Beroud C, Soussi T (2003) The UMD-p53 database: new mutations and analysis tools. Hum Mutat 21(3):176–181
4. Olivier M, Eeles R, Hollstein M, Khan MA, Harries CC, Hainaut P (2002) The IARC TP53 database: new online mutation analysis and recommendations to users. Hum Mutat 19(6):607–614
5. Hainaut P, Hollstein M (2000) p53 and human cancer: the first ten thousand mutations. Adv Cancer Res 77:81–137
6. Hamroun D, Kato S, Ishioka C, Claustars M, Beroud C, Soussi T (2006) The UMD TP53 database and website: update and revisions. Hum Mutat 27(1):14–20
7. Cheok CF, Verma CS, Baselga J, Lane DP (2011) Translating p53 into the clinic. Nat Rev Clin Oncol 8(1):25–37
8. Joerger AC, Fersht AR (2008) Structural biology of the tumor suppressor p53. Annu Rev Biochem 77:557–582
9. Butler JS, Loh SN (2003) Structure, function, and aggregation of the zinc-free form of the p53 DNA binding domain. Biochemistry 42(8): 2396–2403
10. Duan J, Nilsson L (2006) Effect of Zn2+ on DNA recognition and stability of the p53 DNA-binding domain. Biochemistry 45:7483–7492
11. Hollstein M, Sidransky D, Vogelstein B, Harris CC (1991) p53 mutations in human cancers. Science 253(5015):49–53
12. Cho Y, Gorina S, Jeffery PD, Pavletich NP (1994) Crystal structure of a p53 tumor suppressor-DNA complex: understanding tumorigenic mutations. Science 265(5170):346–355
13. Hollstein M, Rice K, Soussi T, Fuchs R, Sorlie T, Hovig E (1994) Smith-SÃ¸rensen B, Montesano R and Harris CC. Database of p53 gene somatic mutations in human tumors and cell lines. Nucleic Acids Res 22(17):3551–3555
14. Greenblatt MS, Bennett WP, Hollstein M, Harris CC (1994) Mutations in the p53 tumor suppressor gene: clues to cancer etiology and molecular pathogenesis. Cancer Res 54:4855–4878
15. Matin AC, Facchiano AM, Cuff AL, Hernandez-Boussard T, Oliver M, Hainaut P, Thornton JM (2002) Integrating mutation data and structural analysis of the TP53 tumor-suppressor protein. Hum Mutat 19(2):149–164
16. Petitjean A, Mathe E, Kato S, Ishioka C, Tavtigian SV, Hainaut P, Olivier M (2007) Impact of mutant p53 functional properties on TP53 mutation patterns and tumor phenotype: lessons from recent developments in the IARC TP53 database. Hum Mutat 28(6):622–9
17. Friedler A, Hansson LO, Veprintsev DB, Freund SM, Rippin TM, Nikolova PV, Proctor MR, Rdiger S, Fersht AR (2002) A peptide that binds and stabilizes p53 core domain: chaperone strategy for rescue of oncogenic mutants. Proc NatlAcad Sci USA 99(2):937–942
18. Bykov VJ, Selivanova G, Wiman KG (2003) Small molecules that reactivate mutant p53. Eur J Cancer 39(13):1829–1834
19. Wiman KG (2006) Strategies for therapeutic targeting of the p53 pathway in cancer. Cell Death Differ 13(6):921–926
20. Bullock AN, Henckel J, DeDecker BS, Johnson CM, Nikolova PV, Proctor MR, Lane DP, Fersht AR (1997) Thermodynamic stability of wild-type and mutant p53 core domain. Proc Natl Acad Sci USA 94(26):14338–14342
21. Bullock AN (2000) Henckel and Fersht AR. Quantitative analysis of residual folding and DNA binding in mutant p53 core domain: definition of mutant states for rescue in cancer therapy. Oncogene 19:1245–1256
22. Cuff AL, Martin AC (2004) Analysis of void volumes in proteins and application to stability of the p53 tumour suppressor protein. J Mol Biol 344:1199–1209
23. Canadillas JM, Tidow H, Freund SM, Rutherford TJ, Ang HC, Fersht AR (2006) Solution structure of p53 core domain: structural basis for its instability. Proc Natl Acad Sci USA 103(7):2109–2114
24. Roth JA (2006) Adenovirus p53 gene therapy. Expert Opin Bio Ther 6(1):55–61
25. Graat HC, Caretee JE, Schagen FH, Vassilev LT, Gerristen WR, Kaspers GJ, Wuisman PI, van Beusechem VW (2007) Enhanced tumor cell kill by combined treatment with a small-molecule antagonist of mouse double minute 2 and adenoviruses encoding p53. Mol Cancer Ther 6(5):1552–1561
26. Wieczorek AM, Waterman JL, Waterman MJ, Halazonetis TD (1996) Structure-based rescue of common tumor-derived p53 mutants. Nat Med 2:1143–1146
27. Brachmann RK, Yu K, Eby Y, Pevletich NP, Boeke JD (1998) Genetic selection of intragenic suppressor mutations that reverse the effect of common p53 cancer mutations. EMBO J 17:1847–1859
28. Nikolova PV, Wong KB, DeDecker B, Henckel J, Fersht AR (2000) Mechanism of rescue of common p53 cancer mutations by second-site suppressor mutations. EMBO J 19:370–378
29. Suad O, Rozenberg H, Brosh R, Diskin-Posner Y, Kessler N, Shimon LJ, Frolow F, Liran A, Rotter V, Shakked Z (2009) Structural basis of restoring sequence-specific DNA binding and transactivation to mutant p53 by suppressor mutations. J Mol Biol 385(1):249–65
30. Baroni TE, Wang T, Qian H, Dearth LR, Truong LN, Zeng J, Denes AE, Chen SW, Brachmann RK (2004) A global suppressor motif for p53 cancer mutants. Proc Natl Acad Sci USA 101:4930–4935
31. Friedler A, DeDecker BS, Freund SMV, Rudiger CBS, Fersht AR (2004) Structural Distortion of p53 by the Mutation R249S and its

Rescue by a Designed Peptide: Implications for Mutant Conformation. J Mol Biol 336:187–196
32. Joerger AC, Allen MD, Fersht AR (2004) Crystal structure of a superstable mutant of human p53 core domain: Insights into the mechanism of rescuing oncogenic mutations. J Biol Chem 279:1291–1296
33. Joerger AC, Ang HC, Veprintsev DB, Blair CM, Fersht AR (2005) Structures of p53 cancer mutants and mechanism of rescue by second-site suppressor mutations. J Biol Chem 280:16030–16037
34. Joerger AC, Ang HC, Fersht AR (2006) Structural basis for understanding oncogenic p53 mutations and designing rescue drugs. Proc Natl Acad Sci USA 103:15056–15061
35. Joerger AC, Fersht AR (2007) Structure-function-rescue: the diverse nature of common p53 cancer mutants. Oncogene 26(15):2226–2242
36. Lu Q, Tan Y-H, Luo R (2007) Molecular dynamics simulations of p53 DNA-binding domain. J Phys Chem B 111(39):11538–11545
37. Barakat K, Issack BB, Stepanova M, Tuszynski J (2011) Effects of temperature on the p53-DNA binding interactions and their dynamical behavior: comparing the wild type to the R248Q mutant. PLoS One 6(11):e27651
38. Benson NC, Daggett V (2012) A comparison of multiscale methods for the analysis of molecular dynamics simulations. J Phys Chem B 116(29):8722–31
39. Wright JD, Noskov SY, Lim C (2002) Factors governing loss and rescue of DNA binding upon single and double mutations in the p53 core domain. Nucleic Acids Res 30:1563–1574
40. Wright JD, Lim C (2007) Mechanism of DNA-binding loss upon single-point mutation in p53. J Biosci 32:827–839
41. Demir O, Baroniao R, Salehi F, Wassman CD, Hall L, Hatfield GW, Chamberlin R, Kaiser P, Lathrop RH, Amaro RE (2011) Ensemble-based computational approach discriminates functional activity of p53 cancer and rescue mutants. Plos Comput Biol 7:e1002238
42. Warshel A, Levitt M (1976) Theoretical Studies of Enzymatic Reactions: Dielectric, Electrostatics and Steric Stabilization of the Carbonium Ion in the Reaction of Lysozyme. J Mol Biol 103:227–249
43. Otsuka K, Kato S, Kakudo Y, Mashiko S, Shibata H, Ishioka C (2007) The screening of the second-site suppressor mutations of the common p53 mutants. Int J Cancer 121:559–566
44. Case DA, Cheatham TE III, Darden T, Gohlke H, Luo R, Merz KM Jr, Onufriev A, Simmerling C, Wang B, Woods RJ (2005) The Amber biomolecular simulation programs. J Comput Chem 26:1668–1688
45. Stewart JJP (1989) Optimization of parameters for semiempirical methods. I Method J Comput Chem 10:209220
46. Ryckaert J-P, Ciccotti G, Berendsen HJC (1977) Numerical integration of the cartesian equations of motion of a system with constraints: Molecular dynamics of n-alkanes. J Comput Phys 23:327341
47. Wu X, Brooks BR (2003) Self-guided Langevin dynamics simulation method. Chem Phys Lett 381:512518
48. Walker RC, Crowley MF, Case DA (2008) The Implementation of a Fast and Accurate QM/MM Potential Method in Amber. J Comput Chem 29(7):1019–31
49. Bakowies D, Thiel W (1996) Hybrid Models for Combined Quantum Mechanical and Molecular Mechanical Approaches. J Phys Chem 100:10580–10594
50. Field MJ, Bash PA, Karplus M (1990) A combined quantum mechanical and molecular mechanical potential for molecular dynamics simulations. J Comput Chem 11(6):700–733
51. Hou T, Wang J, Li Y, Wang W (2011) Assessing the performance of the MM/PBSA and MM/GBSA methods: The accuracy of binding free energy calculations based on molecular dynamics simulations. J Chem Inf Model 51(1):69–82
52. Friedlander P, Legros Y, Soussi T, Prives C (1996) Regulation of mutant p53 temperature-sensitive DNA binding. J Biol Chem 271(11):25468–25478